

CADRef: Robust Out-of-Distribution Detection via Class-Aware Decoupled Relative Feature Leveraging

Zhiwei Ling Yachen Chang Hailiang Zhao* Xinkui Zhao Kingsum Chow
 Shuiguang Deng
 Zhejiang University

{zwl, yachenchang, hliangzhao, zhaoxinkui, kingsum.chow, dengsg}@zju.edu.cn

Abstract

Deep neural networks (DNNs) have been widely criticized for their overconfidence when dealing with out-of-distribution (OOD) samples, highlighting the critical need for effective OOD detection to ensure the safe deployment of DNNs in real-world settings. Existing post-hoc OOD detection methods primarily enhance the discriminative power of logit-based approaches by reshaping sample features, yet they often neglect critical information inherent in the features themselves. In this paper, we propose the Class-Aware Relative Feature-based method (CARef), which utilizes the error between a sample’s feature and its class-aware average feature as a discriminative criterion. To further refine this approach, we introduce the Class-Aware Decoupled Relative Feature-based method (CADRef), which decouples sample features based on the alignment of signs between the relative feature and corresponding model weights, enhancing the discriminative capabilities of CARef. Extensive experimental results across multiple datasets and models demonstrate that both proposed methods exhibit effectiveness and robustness in OOD detection compared to state-of-the-art methods. Specifically, our two methods outperform the best baseline by 2.82% and 3.27% in AUROC, with improvements of 4.03% and 6.32% in FPR95, respectively.

1. Introduction

The remarkable progress in DNNs over the past few years has expanded their application across various domains [11, 22, 24]. However, this success brings an equally significant challenge in terms of model reliability and safety. When exposed to out-of-distribution (OOD) samples, DNNs deployed in real-world settings frequently produce confidently incorrect predictions, failing to recognize when samples fall outside their classification capabilities [13, 25, 32]. This vulnerability introduces substantial risks in safety-critical

*Corresponding author.

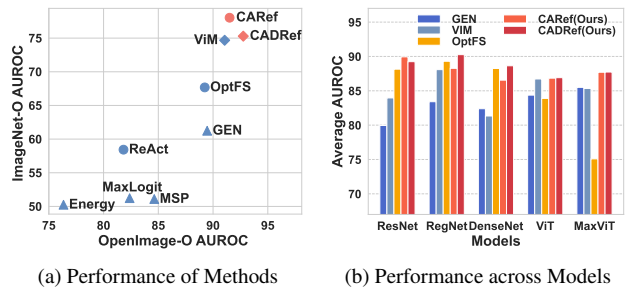


Figure 1. Performance of post-hoc OOD detection methods: (a) shows the average AUROC of various methods tested on the ImageNet-O and OpenImage-O datasets, where \triangle , \circ , and \diamond represent logit-based methods, feature-based methods, and methods that fuse logits and features, respectively. (b) presents the average AUROC of our methods compared to three SOTA methods across different model architectures on the ImageNet-1k benchmark.

fields, such as autonomous driving [15] and medical diagnostics [16], where incorrect predictions could lead to severe consequences. A trustworthy DNN model must not only achieve high accuracy on in-distribution (ID) samples but also effectively identify and reject OOD samples [45, 48]. Therefore, the development of robust OOD detection methods has become an urgent priority for ensuring the safe deployment of DNNs [2, 19].

Currently, the prevailing approach to OOD detection involves designing a post-hoc score function that assigns confidence scores to samples, where ID samples receive high scores, and OOD samples receive low scores to enable clear differentiation [10, 26, 35, 51]. Literature on post-hoc OOD detection can be categorized into two main types: **Logit-based** methods and **Feature-based** methods [3, 5, 30, 49]. As illustrated in Figure 1a, feature-based methods generally outperform logit-based methods to a certain extent, indicating a performance gap. However, Figure 1b shows that logit-based methods can achieve superior results on a few specific models. Despite the effectiveness of feature-based methods, they primarily focus on reshaping features and subsequently adjusting logits, often neglecting the rich in-

formation embedded within the features. This raises an important question: *Can OOD detection methods be designed to integrate both features and logits while fully leveraging the information inherent in sample features?*

In this paper, we introduce a novel OOD detection algorithm called Class-Aware Relative Feature Leveraging (*CARef*). Unlike other feature-based OOD detection methods, our approach specifically focuses on the rich information embedded within sample features. *CARef* first aggregates the sample features in the ID training dataset by class to obtain the average features for each class. For a given test sample, we then compute the relative error between its features and the class-specific average features to determine whether it is an OOD sample. To establish a connection with logits, we further extend *CARef* to the Class-Aware Decoupled Relative Feature (*CADRef*) method, which decouples the sample’s relative features into two components. This decoupling is based on the sign alignment between the relative features and corresponding model weights according to their contribution to the maximum logit. *CADRef* also incorporates advanced logit-based scoring methods to scale the relative errors of these two components, effectively amplifying the distinction between ID and OOD samples. In summary, this paper makes the following three key contributions:

- From the perspective of class-specific feature discrepancy, we propose a simple yet effective OOD detection method, *CARef*, which calculates the relative error of a sample’s features in relation to class-aware features to determine the OOD score.
- By leveraging the association between logits and features, we extend *CARef* to *CADRef*, decoupling sample features based on the alignment of signs between relative features and corresponding model weights. This extension also integrates logit-based OOD detection methods to scale positive errors.
- Comprehensive experimental results across multiple datasets and architectures demonstrate that our methods achieve notable improvements while consistently exhibiting robustness across different architectures.

The rest of this paper is organized as follows: Section 2 provides a brief overview of the preliminaries in OOD detection. Section 3 reviews the related OOD detection methods. Section 4 describes the design of our proposed methods (*CARef* & *CADRef*), and Section 5 presents the experimental results. Finally, Section 6 concludes the paper.

2. Preliminaries

Consider a sample classification task with c classes. Given a DNN model $\mathcal{M} : \mathcal{X} \rightarrow \mathbb{R}^c$ trained on an ID training dataset $\mathcal{D}_{\text{train}}$, the prediction label for any sample $x \in \mathcal{D}_{\text{test}}$ is given by $y = \arg \max_i \mathcal{M}(x)_i$. We further define $\mathcal{F} : \mathcal{X} \rightarrow \mathbb{R}^d$ as the feature extractor, where $\mathcal{F}(x)$ represents

the feature vector from the penultimate layer for the input x . Additionally, let $\mathcal{W} : \mathbb{R}^d \rightarrow \mathbb{R}^c$ and $\mathcal{B} : \mathbb{R}^c \rightarrow \mathbb{R}^c$ denote the weights and biases of the classifier, respectively. The logits \mathcal{L} produced by the model for sample x are computed as follows:

$$\mathcal{L} = \mathcal{M}(x) = \mathcal{W} \cdot \mathcal{F}(x) + \mathcal{B}, \quad (1)$$

$$\mathcal{T} = \arg \max_i \mathcal{M}(x)_i. \quad (2)$$

Let \mathcal{D}_I denote the ID dataset, while \mathcal{D}_O stands for the OOD dataset. The goal of OOD detection is to determine whether a given sample originates from the in-distribution dataset \mathcal{D}_I or the out-of-distribution dataset \mathcal{D}_O , effectively framing it as a binary classification task. This task is based on a scoring function $\text{SCORE}(\cdot; \cdot)$:

$$\begin{cases} x \sim \mathcal{D}_O, & \text{if } \text{SCORE}(\mathcal{M}; x) \leq \gamma, \\ x \sim \mathcal{D}_I, & \text{if } \text{SCORE}(\mathcal{M}; x) > \gamma, \end{cases} \quad (3)$$

where γ is the threshold. According to (3), a sample is classified as an OOD sample if its score falls below γ ; otherwise, it is classified as an ID sample. In real-world applications, once a sample is identified as an OOD sample, the DNN should abstain from making any predictions for it.

3. Related Work

The design of post-hoc OOD score can be categorized into Logits-based ($\mathcal{S}_{\text{logit}}$) and Features-based ($\mathcal{S}_{\text{feature}}$) methods.

3.1. Logit-based OOD-Detection Method

Method	Score Equation
<i>MSP</i> [13]	$\max(\text{SoftMax}(\mathcal{L}))$
<i>MaxLogit</i> [12]	$\max(\mathcal{L})$
<i>ODIN</i> [25]	$\max(\text{SoftMax}(\tilde{\mathcal{L}}))$
<i>Energy</i> [26]	$T \cdot \log \sum (\exp(\mathcal{L}/T))$
<i>GEN</i> [27]	$-\sum_{i=1}^M p_i^\gamma (1 - p_i)^\gamma$

Table 1. Score equations of logit-based OOD-detection methods

Logit-based methods analyze the logits produced by the model for each sample and design confidence scores such that in-distribution (ID) samples yield higher scores while OOD samples yield lower scores [13, 41, 50]. For example, Hendrycks *et al.* propose the classic baseline method, *MSP* [13], which uses the maximum value of the logits after applying the softmax function. Additionally, *ODIN* [25] enhances detection by using temperature scaling and adding small perturbations to the input. Both *Energy* [26] and *GEN* [27] leverage the energy function and generalized entropy, respectively, to construct OOD scores, achieving notable improvements. For large-scale anomaly segmentation tasks,

Hendrycks *et al.* observed that using maximum logits can yield superior performance [12]. Table 1 summarizes the scoring equations for these methods.

3.2. Feature-based OOD-Detection Method

Method	Score Equation
<i>ReAct</i> [35]	$\mathcal{S}_{\text{logit}}(\mathcal{W} \cdot \min(\mathcal{F}(x), \tau) + \mathcal{B})$
<i>DICE</i> [36]	$\mathcal{S}_{\text{logit}}((\mathcal{W} \odot \mathcal{M}) \cdot \mathcal{F}(x) + \mathcal{B})$
<i>ViM</i> [40]	$-\alpha \ \mathcal{F}(x)^{P^\perp}\ _2 + \mathcal{S}_{\text{logit}}(\mathcal{L})$
<i>ASH-S</i> [8]	$\mathcal{S}_{\text{logit}}(\mathcal{W} \cdot (a_s \odot \mathcal{F}(x)) + \mathcal{B})$
<i>ASH-P</i> [8]	$\mathcal{S}_{\text{logit}}(\mathcal{W} \cdot (a_p \odot \mathcal{F}(x)) + \mathcal{B})$
<i>ASH-B</i> [8]	$\mathcal{S}_{\text{logit}}(\mathcal{W} \cdot (a_b \odot \mathcal{F}(x)) + \mathcal{B})$
<i>OptFS</i> [51]	$\mathcal{S}_{\text{logit}}(\mathcal{W} \cdot (\theta \odot \mathcal{F}(x)) + \mathcal{B})$

Table 2. Score equations of feature-based OOD-detection methods

Feature-based methods operate on the feature layer, often by computing or modifying elements in the feature space [1, 20, 23, 35]. These approaches are founded on observing and exploiting the comparative stability of feature behaviors in ID samples relative to OOD samples, thereby enhancing the discriminative gap between ID and OOD samples. For example, *ReAct* [35] removes outliers by truncating features that exceed a certain threshold τ . Djuricic *et al.* [8] introduce a straightforward method that removes most of a sample’s features while applying adjustments to the remaining ones. Their method includes three variants, *ASH-S*, *ASH-P*, and *ASH-B*, which apply different masks to features. These masks are defined as follows:

$$a_s, a_p, a_b = \begin{cases} \exp(\frac{s_o}{s_p}), 1, \frac{s_o}{n \cdot \mathcal{F}(x)_i}, & \text{if } \mathcal{F}(x)_i \geq \tau, \\ 0, & \text{if } \mathcal{F}(x)_i < \tau, \end{cases} \quad (4)$$

where s_o and s_p denote the sum of features before and after pruning, and n represents the number of features retained. *Scale* [43] makes a slight modification to *ASH-S* by retaining pruned features. Moving away from heuristic masks, Zhao *et al.* reformulate feature-shaping masks as an optimization problem [51], where the objective is to maximize the highest logit values for training samples. *DICE* [36] ranks weights according to their contributions on the ID training dataset, pruning those with lower values. In contrast, *ViM* [40] captures the deviation of features from the principal subspace P , making full use of the information embedded in the features. *ViM* [40] also includes the logits associated with ID classes, addressing part of the issues we identified. Table 2 summarizes these feature-based methods.

4. Approach

In this section, we first introduce *CARef* in Subsection 4.1, which is designed to compute class-aware relative feature

errors. Following this, we extend *CARef* to *CADRef* by introducing two essential modules: *Feature Decoupling* and *Error Scaling*.

To achieve a fine-grained decoupling, we separate a sample’s features into positive and negative components based on their contribution to the maximum logit. By analyzing the two resulting error components, *CADRef* effectively mitigates the positive errors of samples with high $\mathcal{S}_{\text{logit}}$ values. Details on these two modules are provided in Subsections 4.2 and 4.3, respectively.

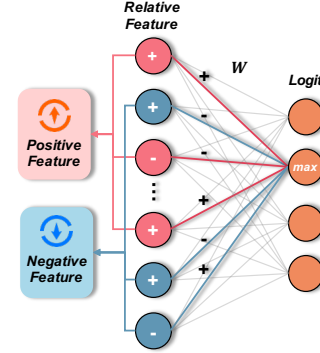


Figure 2. Example diagram of *Feature Decoupling* operation of *CADRef*. Relative features refer to the gap between sample features and class-aware average features. The symbols + and - denote the sign of the corresponding values.

4.1. Class-Aware Relative Feature Error

We begin by extracting the features of the training samples, similar to other feature-based methods [35, 36, 51]. The key difference in our approach is that we group these features based on the predicted labels of the samples and compute the average feature vector for each class. For each $k \in \{1, 2, \dots, c\}$, we define

$$\bar{\mathcal{F}}^k = \frac{1}{n_k} \cdot \sum_{x \in \mathcal{D}_{\text{train}}} \mathbf{1}(\mathcal{T}(x) = k) \cdot \mathcal{F}(x), \quad (5)$$

where n_k is the number of samples with label k in $\mathcal{D}_{\text{train}}$ and $\mathbf{1}(\cdot)$ is the indicator function.

To measure the deviation of individual sample features from their class averages, we propose calculating the relative error between a sample’s feature vector and its corresponding class centroid. Specifically, we compute the normalized l_1 -distance between the sample feature and the average feature, with normalization performed by the l_1 -norm of the sample feature. The error formula and score function for *CARef* are defined as:

$$\mathcal{E}(x) = \frac{\|\mathcal{F}(x) - \bar{\mathcal{F}}^{\mathcal{T}(x)}\|_1}{\|\mathcal{F}(x)\|_1}, \quad \text{SCORE}_{\text{CARef}} = -\mathcal{E}(x). \quad (6)$$

Our experimental results, presented in Table 3 and Table 4,

demonstrate that using class-aware relative feature error as a score function yields remarkable effectiveness.

4.2. Feature Decoupling

As noted in [40], relying solely on sample features limits the effectiveness of OOD detection methods. To address this, we explore the relationship between features and logits in depth and conduct a fine-grained analysis of the features, which distinguishes *CADRef* from *CARef*. Based on an empirical observation, increasing the *maximum* logit (i.e., $\max(\mathcal{L})$) of a sample tends to improve the performance of most logits-based methods. Therefore, we focus on the change in the maximum logit of the sample features relative to the class-aware average features.

Let \mathcal{W}^{\max} denote the weights corresponding to the maximum logit. As illustrated in Figure 2, the contribution to logit values depends on the alignment of signs between the weights and relative features. Specifically, a positive contribution to the maximum logit occurs only when the signs of weights and relative features align, while a mismatch in signs results in an antagonistic effect that diminishes the logit value. By influencing the maximum logit, these positive features also affect logit-based detection methods. We will analyze this relationship further in the next subsection.

Furthermore, the features of each sample can be divided into two parts: POS = $\{i \mid \mathcal{W}_i^{\max} \cdot \mathcal{F}(x)_i > 0\}$ and NEG = $\{i \mid \mathcal{W}_i^{\max} \cdot \mathcal{F}(x)_i < 0\}$. The corresponding errors for these two parts are as follows:

$$\mathcal{E}_p(x) = \frac{\|\sum_{i \in \text{POS}} (\mathcal{F}(x)_i - \bar{\mathcal{F}}_i^T(x))\|_1}{\|\mathcal{F}(x)\|_1}, \quad (7)$$

$$\mathcal{E}_n(x) = \frac{\|\sum_{i \in \text{NEG}} (\mathcal{F}(x)_i - \bar{\mathcal{F}}_i^T(x))\|_1}{\|\mathcal{F}(x)\|_1}. \quad (8)$$

4.3. Error Scaling

Decomposing $\mathcal{E}(x)$ into $\mathcal{E}_p(x)$ and $\mathcal{E}_n(x)$ does not impact the relative error between samples. To investigate their individual contributions, we evaluated these components separately as OOD detection scores. Empirical results show that, compared to *CARef*, using the positive error as the score substantially reduces OOD detection performance, while using the negative error as the score achieves nearly comparable performance. As shown in Figure 3, the AUROC and FPR95 of \mathcal{E}_p are approximately 13% and 15% lower than those of *CARef*, respectively. In contrast, \mathcal{E}_n shows a 2.03% and 7.00% increase. Due to the poor classification performance of the positive error, we conclude that it plays a harmful role in *CARef*'s coupling form, highlighting the need to focus on enhancing \mathcal{E}_p .

Since \mathcal{E}_p is closely related to logit-based methods, we explore the relationship between S_{logit} and \mathcal{E}_p for a sample, using the *Energy* [26] and *GEN* [27] scores as examples.

Results for other methods are provided in the supplementary materials. As shown in Figure 4a and Figure 4c, we observe that \mathcal{E}_p effectively distinguishes between ID and OOD samples at lower S_{logit} values. However, at higher S_{logit} values, \mathcal{E}_p for ID and OOD samples shows substantial overlap, which reduces OOD detection performance. To address this issue, we propose *using the ratio of \mathcal{E}_p to S_{logit} instead of \mathcal{E}_p alone*. When ID and OOD samples have similar \mathcal{E}_p values, the higher S_{logit} of ID samples reduces this ratio, while for OOD samples, the effect is reversed. For the negative error, as shown in Figure 4b and Figure 4d, we observe the opposite phenomenon. There is no overlap in \mathcal{E}_n between ID and OOD samples at high S_{logit} , while some overlap exists at low S_{logit} . This overlap does not impact the detection performance of the negative error, as low S_{logit} values indicate that distinguishing these samples is challenging for any detection method. Therefore, modifying the negative error is deemed unnecessary for performance enhancement.

Comparing Figure 3c with Figure 3d, we can find that scaling the positive error significantly enhances the separation between ID and OOD samples. Finally, we consider a fusion form of the positive and negative errors. To ensure consistency in the magnitude of both errors, we also apply a constant decay to the negative error, with the constant term set to the average score of all ID training samples:

$$\bar{S}_{\text{logit}} = \frac{1}{n} \cdot \sum_{x \in \mathcal{D}_{\text{train}}} S_{\text{logit}}(x). \quad (9)$$

The final score formula of our *CADRef* is as follows:

$$\mathcal{E}(x) = \frac{\mathcal{E}_p(x)}{S_{\text{logit}}(x)} + \frac{\mathcal{E}_n(x)}{\bar{S}_{\text{logit}}}, \quad \text{SCORE}_{\text{CADRef}} = -\mathcal{E}(x). \quad (10)$$

As shown in Figure 3e, the fusion of both errors further enhances the distinction between ID and OOD samples compared to using each error individually.

5. Experiments

In this section, we conduct extensive experiments across multiple datasets and models to evaluate the performance of our two methods, and compare them with state-of-the-art OOD detection methods, all of which are implemented by PyTorch [33].

5.1. Setup

Datasets. We conduct experiments on both large-scale and small-scale benchmarks. For the large-scale benchmark, we use ImageNet-1k [7] as the in-distribution (ID) dataset and evaluate performance across six commonly used OOD datasets: iNaturalist [17], SUN [42], Places [52], Texture [6], OpenImage-O [40], and ImageNet-O [14]. For the small-scale benchmark, we use CIFAR-10 [21] and CIFAR-100 [21] as ID datasets, with performance evaluated on six

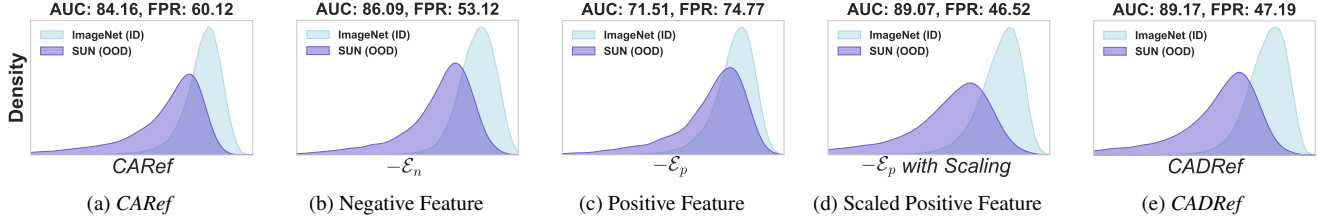


Figure 3. Detection results and score distributions on ImageNet-1k (blue) [7] and SUN (purple) [42] using DenseNet-201 [11].

Method	ResNet		RegNet		DenseNet		ViT		Swin		ConvNeXt		MaxViT		Average	
	AU \uparrow	FP \downarrow	AU \uparrow	FP \downarrow	AU \uparrow	FP \downarrow	AU \uparrow	FP \downarrow	AU \uparrow	FP \downarrow	AU \uparrow	FP \downarrow	AU \uparrow	FP \downarrow	AU \uparrow	FP \downarrow
<i>MSP</i> [13]	74.14	70.44	78.34	69.98	77.76	67.63	79.33	66.29	77.81	67.12	76.23	65.24	80.36	63.50	77.71	67.17
<i>MaxLogit</i> [12]	79.64	65.00	81.71	63.75	81.16	61.56	75.68	65.40	70.85	67.68	68.76	72.66	77.18	57.28	76.43	64.76
<i>ODIN</i> [25]	79.28	60.32	80.57	58.66	78.90	60.75	61.45	94.33	55.22	91.02	51.09	89.33	64.60	81.46	67.30	76.55
<i>Energy</i> [26]	79.85	64.53	81.55	64.11	81.09	61.25	71.04	70.23	63.18	75.96	52.91	91.09	73.01	62.46	71.80	69.95
<i>GEN</i> [27]	79.95	66.70	83.41	63.46	82.39	63.01	84.37	<u>59.58</u>	83.72	55.33	82.69	<u>54.90</u>	85.50	51.22	83.15	59.17
<i>ReAct</i> [35]	86.03	44.09	86.62	46.30	78.46	64.18	79.65	69.99	81.91	66.57	78.15	76.87	63.78	78.91	79.23	63.84
<i>DICE</i> [36]	82.48	47.90	77.92	68.89	79.20	59.04	71.65	88.51	45.79	86.76	45.12	89.77	63.20	76.78	66.48	73.95
<i>ASH-S</i> [8]	90.11	35.52	<u>89.37</u>	38.01	87.56	43.80	18.06	99.62	19.18	99.35	20.30	98.23	55.26	86.30	54.26	71.55
<i>OptFS</i> [51]	88.15	42.47	89.30	42.97	<u>88.25</u>	47.88	83.89	65.99	84.71	65.03	85.06	61.17	75.09	70.84	84.92	56.62
<i>ViM</i> [40]	83.96	65.85	88.08	56.13	81.33	72.66	86.72	49.36	83.96	63.63	84.24	58.57	85.34	53.56	84.80	59.97
<i>CARef</i>	<u>89.94</u>	40.91	88.27	50.68	86.55	52.59	<u>86.84</u>	60.48	<u>86.92</u>	58.65	87.95	54.09	<u>87.70</u>	<u>50.75</u>	<u>87.74</u>	<u>52.59</u>
<i>CADRef</i>	89.24	<u>40.68</u>	90.26	<u>42.34</u>	88.64	<u>45.25</u>	86.91	60.05	87.10	<u>57.38</u>	87.48	56.92	87.73	49.49	88.19	50.30

Table 3. Results of OOD detection on ImageNet-1k benchmark. \uparrow indicates that higher values are better, while \downarrow indicates that lower values are better. All values are percentages, with the best and second-best results being **highlighted** and underlined, respectively.

widely used OOD datasets: SVHN [31], LSUN-Crop [46], LSUN-Resize [46], iSUN [44], Texture [6], and Places [52]. All OOD datasets have been resized to match the dimensions of the ID datasets.

Models architectures. To validate the robustness of the proposed methods, we conduct experiments using several well-known model architectures, including convolutional neural networks (CNNs) and vision transformers. For ImageNet-1k, we use four representative CNN-based models: ResNet-50 [11], RegNetX-8GF [34], DenseNet-201 [18], and ConvNeXt-B [29], as well as three transformer-based models: ViT-B/16 [9], Swin-B [28], and MaxViT-T [38] to ensure a comprehensive evaluation. The pre-trained model weights are sourced from the PyTorch model zoo [33]. For experiments on CIFAR-10 and CIFAR-100, we use DenseNet-101 [18] with pre-trained weights provided by prior work [36].

Baselines. We evaluate our two proposed methods, with *CADRef* leveraging the *Energy* [26] score as the source for

Error Scaling. For comparison, we implement ten baseline methods for OOD detection, covering both logit-based and feature-based approaches. The logit-based methods include *MSP* [13], *MaxLogit* [12], *ODIN* [25], *Energy* [26] and *GEN* [27]. Meanwhile, the feature-based methods comprise *ReAct* [35], *DICE* [36], *ASH-S* [8], *OptFS* [51] and *ViM* [40]. Note that all feature-based methods use *energy* as the score function. Details of the hyperparameters for each baseline are provided in the *supplementary materials*.

Evaluation metrics. We evaluate the OOD detection performance using two standard metrics, consistent with prior works [13, 37]: area under the receiver operating characteristic curve (AUROC) and false positive rate at a true positive rate of 95% (FPR95). Higher AUROC values and lower FPR95 values indicate better OOD detection performance.

5.2. Comparison with SOTA Methods

On ImageNet-1k Benchmark. Table 3 presents the experimental results on ImageNet-1k. We also provide de-

Methods	SVHN		LSUN-C		LSUN-R		iSUN		Textures		Places		Average		
	AU \uparrow	FP \downarrow	AU \uparrow	FP \downarrow	AU \uparrow	FP \downarrow	AU \uparrow	FP \downarrow	AU \uparrow	FP \downarrow	AU \uparrow	FP \downarrow	AU \uparrow	FP \downarrow	
CIFAR-10	<i>MSP</i> [13]	93.56	47.19	93.42	47.09	94.54	42.07	94.49	42.53	88.24	63.88	90.02	60.01	92.38	50.46
	<i>MaxLogit</i> [12]	94.32	37.79	97.22	16.31	98.12	9.41	98.05	10.08	86.65	56.57	93.61	34.82	94.66	27.50
	<i>ODIN</i> [25]	92.88	39.95	96.02	21.34	99.29	3.09	99.19	3.79	86.16	53.22	92.57	38.81	94.35	26.70
	<i>Energy</i> [26]	94.19	38.71	97.29	15.55	98.18	8.70	98.11	9.42	86.56	56.66	93.67	33.92	94.67	27.16
	<i>GEN</i> [27]	95.19	30.75	96.99	18.29	97.93	11.29	97.87	11.93	88.87	54.00	93.34	36.30	95.03	27.09
	<i>ReAct</i> [35]	66.05	97.18	78.03	87.24	84.86	71.13	83.77	73.66	68.08	90.85	75.53	83.72	76.05	83.96
	<i>DICE</i> [36]	94.96	27.74	<u>98.31</u>	<u>8.86</u>	99.05	4.22	98.99	5.16	87.33	45.33	93.86	31.84	95.42	20.52
	<i>ASH-S</i> [8]	98.73	6.16	98.13	9.67	98.91	4.84	98.87	5.13	95.29	23.58	93.58	<u>32.32</u>	<u>97.25</u>	<u>13.62</u>
	<i>OptFS</i> [51]	96.01	24.35	96.99	18.09	98.11	9.31	98.00	10.25	94.29	32.96	92.33	40.15	95.95	22.52
	<i>ViM</i> [40]	98.45	8.65	97.36	15.39	<u>99.28</u>	<u>3.17</u>	99.12	4.50	96.18	20.33	89.80	54.48	96.70	17.75
<i>CARef</i>	<u>99.11</u>	<u>4.66</u>	98.22	9.51	98.93	5.20	98.77	6.11	96.79	16.29	91.59	41.19	97.23	13.83	
<i>CADRef</i>	99.17	4.16	98.66	7.02	99.23	3.61	<u>99.13</u>	<u>4.34</u>	<u>96.71</u>	<u>17.52</u>	<u>93.72</u>	<u>32.74</u>	97.77	11.56	
CIFAR-100	<i>MSP</i> [13]	75.19	82.02	78.63	76.44	67.13	87.28	68.49	88.00	71.20	85.19	70.84	85.28	71.91	84.04
	<i>MaxLogit</i> [12]	81.42	86.17	87.90	58.91	77.41	76.05	76.54	79.13	71.14	84.45	76.18	79.82	78.43	77.42
	<i>ODIN</i> [25]	80.33	86.53	89.10	51.85	86.41	56.66	85.78	59.03	73.57	80.49	76.83	79.80	82.00	69.06
	<i>Energy</i> [26]	81.30	88.03	88.11	58.19	77.77	75.17	76.79	78.61	70.99	85.00	76.21	79.95	78.53	77.49
	<i>GEN</i> [27]	80.97	78.89	83.72	70.82	71.51	84.11	72.00	85.15	74.26	83.68	73.88	83.36	76.06	81.00
	<i>ReAct</i> [35]	69.13	96.75	78.84	77.21	86.44	68.03	82.86	74.78	67.15	92.07	59.99	89.72	74.07	83.09
	<i>DICE</i> [36]	88.18	60.06	92.98	36.40	88.23	55.03	88.50	52.49	77.22	61.27	81.18	73.89	86.05	56.52
	<i>ASH-S</i> [8]	95.79	24.75	<u>94.14</u>	<u>29.98</u>	89.54	54.06	90.93	48.15	92.11	34.60	<u>79.22</u>	<u>76.96</u>	90.29	44.75
	<i>OptFS</i> [51]	84.96	73.61	90.01	47.98	83.61	69.52	84.39	70.56	85.63	61.64	74.37	80.96	83.83	67.38
	<i>ViM</i> [40]	93.57	35.05	92.76	40.06	95.50	24.65	95.63	23.22	95.89	19.75	75.61	83.89	91.49	37.77
<i>CARef</i>	96.83	17.41	90.96	40.74	89.25	52.69	91.08	45.32	93.99	<u>25.48</u>	67.92	88.30	88.34	44.99	
<i>CADRef</i>	<u>96.69</u>	<u>18.28</u>	94.70	27.22	<u>90.26</u>	<u>47.45</u>	<u>91.59</u>	<u>42.10</u>	<u>94.13</u>	<u>28.72</u>	75.91	78.30	<u>90.55</u>	<u>40.34</u>	

Table 4. Results of OOD detection on CIFAR benchmarks. \uparrow indicates that higher values are better, while \downarrow indicates that lower values are better. All values are percentages, with the best and second-best results being **highlighted** and underlined, respectively.

tailed results for all datasets in the *supplementary materials*. From the average results among all models, both *CARef* and *CADRef* remain in the top two positions. Compared to the best baseline, *CADRef* improves the AUROC by 3.27% and reduces the FPR95 by 6.32%, while *CARef* also improves the AUROC by 2.82% and reduces the FPR95 by 4.03%. We group the baselines for detailed analysis:

- **vs. feature shaping-based methods:** Experimental results demonstrate that feature shaping-based methods exhibit strong performance on specific architectures, notably ResNet-50, RegNetX-8GF, and DenseNet-201. For example, *ASH-S* achieves state-of-the-art performance on ResNet-50 and reports the lowest FPR95 values on both RegNetX-8GF and DenseNet-201. However, for other model architectures, the performance of these meth-

ods significantly declines, with the *ASH-S* method even collapsing (AUROC below 50% on ViT-B/16, Swin-B, and ConvNeXt-B). This observation indicates that feature shaping-based methods exhibit architecture-specific behavior and lack cross-model robustness. In contrast, our methods demonstrate outstanding performance on individual models, almost always ranking in the top two, further highlighting the robustness. To address the issue of performance collapse, *OptFS* discards the heuristic mask design based on empirical methods and instead focuses on automating the optimization of masks across different models. While *OptFS* substantially improves cross-architecture robustness, as evidenced in Table 3, its performance remains inferior to both *CARef* and *CADRef*.

- **vs. logit-based methods:** According to the Table 3, com-

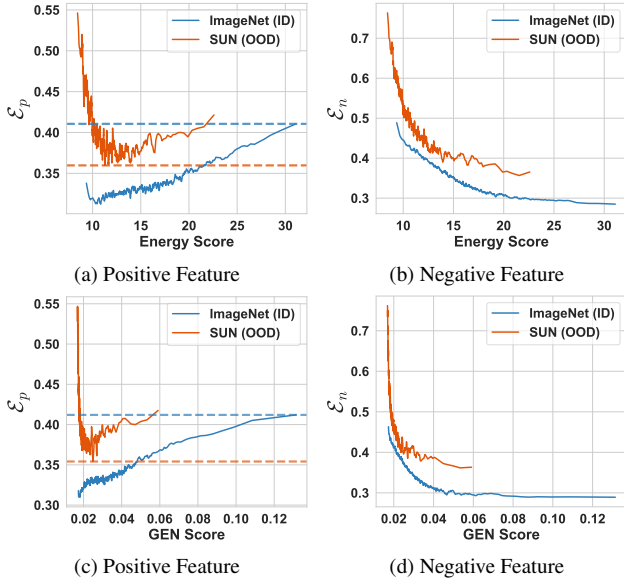


Figure 4. Score and error distribution of ID/OOD samples.

pared to feature shaping-based methods, most logit-based methods do not perform well, except for *GEN*. However, these methods do not suffer from similar collapses on certain models as feature shaping-based methods, making them more generalizable compromise solutions. Additionally, logit-based methods do not require extra ID training data, which gives them an advantage in terms of computational resources.

- **vs. ViM:** We focus especially on the comparison with *ViM*, since it similarly utilizes feature information and logit-based scores, making it a method of the same category as *CADRef*. As shown in the Table 3, *CADRef* outperforms *ViM* in all other cases except for the FPR95 on ViT-B/16. On DenseNet, the fact that the effect of *ViM* is closely approximated by *Energy* (logit-based component) suggests that *ViM* does not fully utilize feature information. Our method demonstrates that, compared to projecting into other spaces, ID and OOD samples exhibit significant separability within the feature space.

On CIFAR Benchmarks. Table 4 also shows the experimental results on CIFAR-10 and CIFAR-100 benchmarks. Our proposed *CADRef* demonstrates superior performance on CIFAR-10, achieving state-of-the-art results, while maintaining competitive performance on CIFAR-100 with only marginal differences from the best baseline method. We also observe a decline in the performance of *CARef* on the CIFAR benchmarks. This phenomenon can be attributed to the reduced feature dimensionality in small-scale datasets, which potentially compromises the precision of relative error calculations.

5.3. Impact of various logit-based methods

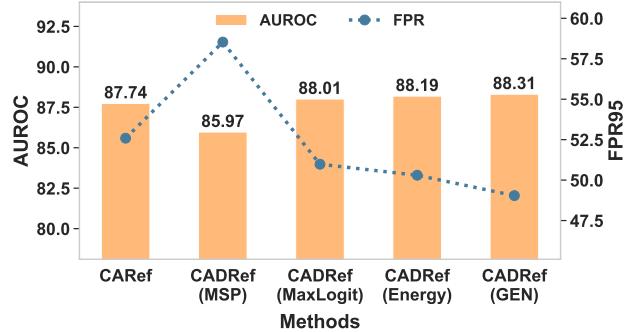


Figure 5. The Impact of various logit-based methods on *CADRef*

Figure 5 provides the performance of *CADRef* on the ImageNet-1k benchmark, using *MSP*, *Maxlogit*, *Energy*, and *GEN* as the logit-based scores, respectively. The results demonstrate that *CADRef+GEN* achieves superior performance in both AUROC and FPR95 metrics among all logit-based variants, which aligns with the exceptional performance of *GEN* previously observed in Table 3. Furthermore, the performance of both *CADRef+MaxLogit* and *CADRef+Energy* surpasses all baselines in Table 3. We also observe an interesting phenomenon in Figure 5 that deserves exploration in future work. Compared to *CARef*, using *MaxLogit*, *Energy*, and *GEN* significantly improves the performance of *CADRef*, while using *MSP* leads to a substantial decline in its performance. This contrasts with the trend observed in the Table 3, where *MSP* demonstrates superior performance over both *MaxLogit* and *Energy*.

5.4. Ablation Study

Architectures	ℓ_1 -Distance		ℓ_1 -Norm		<i>CARef</i>	
	AU \uparrow	FP \downarrow	AU \uparrow	FP \downarrow	AU \uparrow	FP \downarrow
ResNet	74.26	78.65	79.69	55.20	89.94	40.91
ViT	85.16	66.11	20.11	99.44	86.84	60.48
Swin	85.83	67.05	15.95	99.75	86.92	58.65
ConvNeXt	87.49	58.54	14.09	99.83	87.95	54.09
DenseNet	69.32	85.54	68.66	75.31	86.55	52.59
RegNet	77.30	76.17	65.36	86.11	88.27	50.68
MaxViT	85.99	64.43	22.12	99.46	87.70	50.75
Average	62.19	80.76	40.85	87.87	87.74	52.59

Table 5. Ablation Study of *CARef*. ℓ_1 -Distance represents the negative of the ℓ_1 distance between the sample feature and the class-aware average feature as the score function, while ℓ_1 -Norm uses the ℓ_1 norm of the sample feature as the score function.

Ablation of *CARef*. In Table 5, we presents the ablation re-

sults of *CARef* on the ImageNet-1k benchmark, with all values averaged across multiple OOD datasets. Experiments show that using either ℓ_1 -Distance or ℓ_1 -Norm alone results in a significant performance gap compared to the baseline. Yu *et al.* observe on ResNet that ID samples generally exhibit a larger feature norm than OOD samples [47]. The ℓ_1 -Norm is similar to their proposed *FeatureNorm*, with the main distinction being that *FeatureNorm* focuses on a specific feature layer block. However, our experiments reveal that this phenomenon does not generalize across different models. Specifically, our experiments with models including ViT, Swin, ConvNeXt, and MaxViT demonstrate contrary behavior, with ℓ_1 -Norm achieving AUROC scores below 30% and FPR95 values exceeding 99%. This suggests that the scoring for ID and OOD samples is reversed, meaning that in most cases, the feature norm of OOD samples is greater than that of ID samples. In contrast, *CARef*, as a combination of both, demonstrates significant performance improvement and robustness across multiple models.

FD	\mathcal{E}_p	\mathcal{E}_n	ES	AU \uparrow	FP \downarrow
\times	—	—	—	87.74	52.59
\checkmark	\checkmark	\times	\times	82.52	65.67
\checkmark	\times	\checkmark	\times	87.70	<u>51.82</u>
\checkmark	\checkmark	\times	\checkmark	87.58	52.43
\checkmark	\checkmark	\checkmark	\checkmark	88.19	50.30

Table 6. Ablation Study of *CADRef*. **FD** and **ES** represent the *Feature Decoupling* and *Error Scaling* components, respectively. \checkmark and \times indicate whether the component is used or not.

Ablation of *CADRef*. As shown in Table 6, we also conduct ablation experiments to verify the effectiveness of each module of *CADRef*. The first and fifth rows show the results for *CARef* and *CADRef*, respectively. The experimental results demonstrate that removing any component results in a degradation in the performance of *CADRef*, which validates that each component plays a crucial role. The second and third rows of the table clearly show that using the negative error significantly outperforms using the positive error. Furthermore, the AUROC result obtained by using the negative error alone is comparable to that of *CARef*, with even a lower FPR95. This suggests that the effect of using the positive error without *Error Scaling* can be considered negligible. However, once *Error Scaling* is applied to the positive error (the fourth row), its performance becomes comparable to that of the negative error. Note that *Error Scaling* cannot be applied independently of *Feature Decoupling*, so we can only validate their collaborative effectiveness, as reflected in the performance gap between *CADRef* and *CARef*.

Methods	ImageNet-O		SSB-hard		Ninco	
	AU \uparrow	FP \downarrow	AU \uparrow	FP \downarrow	AU \uparrow	FP \downarrow
<i>Energy</i> [26]	50.25	92.71	66.99	83.40	72.41	76.59
<i>Residual</i> [40]	76.37	78.99	57.06	89.05	70.47	80.18
<i>ViM</i> [40]	74.68	82.14	68.81	85.16	81.72	71.51
<i>CARef</i>	78.03	81.73	72.32	81.04	83.65	68.27
<i>CADRef</i>	75.29	85.21	74.58	78.79	85.36	64.89

Table 7. The effect of the logit-based scoring component on *CADRef* and *ViM* on three hard OOD dataset. Both *CADRef* and *ViM* use *Energy* as their logit-based component.

5.5. Discussion

In this subsection, we examine the limitations of *CADRef*'s logit-based component through experiments on three hard OOD benchmarks: ImageNet-O [14], SSB-hard [39], and Ninco [4], which have been empirically shown to be challenging for logit-based methods. Additionally, we also include a comparative analysis between *ViM* and its feature-only component, *Residual* [40]. As shown in Table 7, the performance of *Energy* on ImageNet-O degrades to an AUROC of approximately 50%, essentially reducing to random classification. This degradation is reflected in both *CADRef* and *ViM*, which underperform their respective feature-only counterparts on this dataset. While SSB-hard and Ninco are also considered hard OOD datasets, *Energy* maintains discriminative capability with AUROC scores above 60%. In these cases, *CADRef* demonstrates superior performance compared to *CARef*, a pattern similarly observed in the comparison between *ViM* and *Residual*. These empirical findings lead to two key conclusions: (1) When logit-based methods encounter catastrophic failure on extremely challenging OOD datasets, their integration into *CADRef* becomes detrimental to overall performance; (2) However, in scenarios where logit-based methods maintain even modest discriminative power, they contribute positively to the effectiveness of *CADRef*.

6. Conclusion

In this paper, we presented a novel OOD detection framework, *CADRef*, which leverages class-aware decoupled relative features to enhance the detection of out-of-distribution samples. Building on the class-aware relative error approach of *CARef*, *CADRef* incorporates feature decoupling and error scaling, allowing for a more nuanced separation of in-distribution and out-of-distribution samples based on their positive and negative feature contributions. Comprehensive experiments across both large-scale and small-scale benchmarks demonstrate the robustness and effectiveness of *CADRef*, particularly when combined with advanced

logit-based scores such as *GEN*, yielding superior AUROC and FPR95 metrics compared to state-of-the-art baselines. Future work may investigate additional decoupling strategies and adaptive scaling techniques to further enhance detection reliability across diverse datasets and architectures.

Acknowledgment

This work was supported in part by the National Key Research and Development Program of China under Grant 2024YFB3309400, the National Science Foundation of China (62125206, 62472375, 62472338), the Major Program of the National Natural Science Foundation of Zhejiang (LD24F020014, LD25F020002), and the Zhejiang Pioneer (Jianbing) Project (2024C01032). Hailiang Zhao’s work was supported in part by the Zhejiang University Education Foundation Qizhen Scholar Foundation.

References

- [1] Yong Hyun Ahn, Gyeong-Moon Park, and Seong Tae Kim. Line: Out-of-distribution detection by leveraging important neurons. In *Conference on Computer Vision and Pattern Recognition (CVPR)*, pages 19852–19862, 2023. 3
- [2] Yichen Bai, Zongbo Han, Bing Cao, Xiaoheng Jiang, Qinghua Hu, and Changqing Zhang. Id-like prompt learning for few-shot out-of-distribution detection. In *Conference on Computer Vision and Pattern Recognition (CVPR)*, pages 17480–17489, 2024. 1
- [3] Sima Behpour, Thang Long Doan, Xin Li, Wenbin He, Liang Gou, and Liu Ren. Gradorth: A simple yet efficient out-of-distribution detection with orthogonal projection of gradients. In *Advances in Neural Information Processing Systems (NeurIPS)*, 2023. 1
- [4] Julian Bitterwolf, Maximilian Müller, and Matthias Hein. In or out? fixing imagenet out-of-distribution detection evaluation. In *International Conference on Machine Learning (ICML)*, volume 202, pages 2471–2506, 2023. 8
- [5] Jिंगgang Chen, Junjie Li, Xiaoyang Qu, Jianzong Wang, Jiguang Wan, and Jing Xiao. GAIA: delving into gradient-based attribution abnormality for out-of-distribution detection. In *Advances in Neural Information Processing Systems (NeurIPS)*, 2023. 1
- [6] Mircea Cimpoi, Subhansu Maji, Iasonas Kokkinos, Sammy Mohamed, and Andrea Vedaldi. Describing textures in the wild. In *Computer Vision and Pattern Recognition (CVPR)*, pages 3606–3613, 2014. 4, 5
- [7] Jia Deng, Wei Dong, Richard Socher, Li-Jia Li, Kai Li, and Li Fei-Fei. Imagenet: A large-scale hierarchical image database. In *Computer Vision and Pattern Recognition (CVPR)*, pages 248–255, 2009. 4, 5
- [8] Andrija Djurisic, Nebojsa Bozanic, Arjun Ashok, and Rosanne Liu. Extremely simple activation shaping for out-of-distribution detection. In *International Conference on Learning Representations (ICLR)*, 2023. 3, 5, 6
- [9] Alexey Dosovitskiy, Lucas Beyer, Alexander Kolesnikov, Dirk Weissenborn, Xiaohua Zhai, Thomas Unterthiner, Mostafa Dehghani, Matthias Minderer, Georg Heigold, Sylvain Gelly, Jakob Uszkoreit, and Neil Houlsby. An image is worth 16x16 words: Transformers for image recognition at scale. In *International Conference on Learning Representations (ICLR)*, 2021. 5
- [10] Ke Fan, Tong Liu, Xingyu Qiu, Yikai Wang, Lian Huai, Zeyu Shangguan, Shuang Gou, Fengjian Liu, Yuqian Fu, Yanwei Fu, and Xingqun Jiang. Test-time linear out-of-distribution detection. In *Computer Vision and Pattern Recognition (CVPR)*, pages 23752–23761, 2024. 1
- [11] Kaiming He, Xiangyu Zhang, Shaoqing Ren, and Jian Sun. Deep residual learning for image recognition. In *Computer Vision and Pattern Recognition (CVPR)*, pages 770–778, 2016. 1, 5
- [12] Dan Hendrycks, Steven Basart, Mantas Mazeika, Andy Zou, Joseph Kwon, Mohammadreza Mostajabi, Jacob Steinhardt, and Dawn Song. Scaling out-of-distribution detection for real-world settings. In *International Conference on Machine Learning (ICML)*, volume 162, pages 8759–8773, 2022. 2, 3, 5, 6
- [13] Dan Hendrycks and Kevin Gimpel. A baseline for detecting misclassified and out-of-distribution examples in neural networks. In *International Conference on Learning Representations (ICLR)*, 2017. 1, 2, 5, 6
- [14] Dan Hendrycks, Kevin Zhao, Steven Basart, Jacob Steinhardt, and Dawn Song. Natural adversarial examples. In *Computer Vision and Pattern Recognition (CVPR)*, pages 15262–15271, 2021. 4, 8
- [15] Jens Henriksson, Christian Berger, Stig Ursing, and Markus Borg. Evaluation of out-of-distribution detection performance on autonomous driving datasets. In *International Conference on Artificial Intelligence Testing (AITest)*, pages 74–81, 2023. 1
- [16] Zesheng Hong, Yubiao Yue, Yubin Chen, Huanjie Lin, Yuanmei Luo, Mini Han Wang, Weidong Wang, Jialong Xu, Xiaoqi Yang, Zhenzhang Li, and Sihong Xie. Out-of-distribution detection in medical image analysis: A survey. *arXiv preprint arXiv:2404.18279*, 2024. 1
- [17] Grant Van Horn, Oisín Mac Aodha, Yang Song, Yin Cui, Chen Sun, Alexander Shepard, Hartwig Adam, Pietro Perona, and Serge J. Belongie. The inaturalist species classification and detection dataset. In *Computer Vision and Pattern Recognition (CVPR)*, pages 8769–8778, 2018. 4
- [18] Gao Huang, Zhuang Liu, Laurens van der Maaten, and Kilian Q. Weinberger. Densely connected convolutional networks. In *Computer Vision and Pattern Recognition (CVPR)*, pages 2261–2269, 2017. 5
- [19] Rui Huang and Yixuan Li. MOS: towards scaling out-of-distribution detection for large semantic space. In *Conference on Computer Vision and Pattern Recognition (CVPR)*, pages 8710–8719, 2021. 1
- [20] Wenyu Jiang, Hao Cheng, Mingcai Chen, Chongjun Wang, and Hongxin Wei. DOS: diverse outlier sampling for out-of-distribution detection. In *International Conference on Learning Representations (ICLR)*, 2024. 3
- [21] Alex Krizhevsky, Geoffrey Hinton, et al. Learning multiple layers of features from tiny images. 2009. 4

- [22] Yann LeCun, Yoshua Bengio, and Geoffrey Hinton. Deep learning. *nature*, 521(7553):436–444, 2015. 1
- [23] Kimin Lee, Kibok Lee, Honglak Lee, and Jinwoo Shin. A simple unified framework for detecting out-of-distribution samples and adversarial attacks. In *Advances in Neural Information Processing Systems (NeurIPS)*, pages 7167–7177, 2018. 3
- [24] Shutao Li, Weiwei Song, Leyuan Fang, Yushi Chen, Pedram Ghamisi, and Jón Atli Benediktsson. Deep learning for hyperspectral image classification: An overview. *IEEE Transactions on Geoscience and Remote Sensing*, 57(9):6690–6709, 2019. 1
- [25] Shiyu Liang, Yixuan Li, and R. Srikant. Enhancing the reliability of out-of-distribution image detection in neural networks. In *International Conference on Learning Representations (ICLR)*, 2018. 1, 2, 5, 6
- [26] Weitang Liu, Xiaoyun Wang, John D. Owens, and Yixuan Li. Energy-based out-of-distribution detection. In *Conference on Neural Information Processing Systems (NeurIPS)*, 2020. 1, 2, 4, 5, 6, 8
- [27] Xixi Liu, Yaroslava Lochman, and Christopher Zach. GEN: pushing the limits of softmax-based out-of-distribution detection. In *Computer Vision and Pattern Recognition (CVPR)*, pages 23946–23955, 2023. 2, 4, 5, 6
- [28] Ze Liu, Yutong Lin, Yue Cao, Han Hu, Yixuan Wei, Zheng Zhang, Stephen Lin, and Baining Guo. Swin transformer: Hierarchical vision transformer using shifted windows. In *International Conference on Computer Vision (ICCV)*, pages 9992–10002, 2021. 5
- [29] Zhuang Liu, Hanzi Mao, Chao-Yuan Wu, Christoph Feichtenhofer, Trevor Darrell, and Saining Xie. A convnet for the 2020s. In *Conference on Computer Vision and Pattern Recognition (CVPR)*, pages 11966–11976, 2022. 5
- [30] Shuo Lu, Yingsheng Wang, Lijun Sheng, Aihua Zheng, Lingxiao He, and Jian Liang. Recent advances in OOD detection: Problems and approaches. *arXiv preprint arXiv:2409.11884*, 2024. 1
- [31] Yuval Netzer, Tao Wang, Adam Coates, Alessandro Bisacco, Baolin Wu, Andrew Y Ng, et al. Reading digits in natural images with unsupervised feature learning. In *NIPS workshop on deep learning and unsupervised feature learning*, volume 2011, page 4, 2011. 5
- [32] Anh Mai Nguyen, Jason Yosinski, and Jeff Clune. Deep neural networks are easily fooled: High confidence predictions for unrecognizable images. In *Computer Vision and Pattern Recognition (CVPR)*, pages 427–436, 2015. 1
- [33] Adam Paszke, Sam Gross, Francisco Massa, Adam Lerer, James Bradbury, Gregory Chanan, Trevor Killeen, Zeming Lin, Natalia Gimelshein, Luca Antiga, Alban Desmaison, Andreas Köpf, Edward Z. Yang, Zachary DeVito, Martin Raison, Alykhan Tejani, Sasank Chilamkurthy, Benoit Steiner, Lu Fang, Junjie Bai, and Soumith Chintala. Pytorch: An imperative style, high-performance deep learning library. In *Proceedings of the Advances in Neural Information Processing Systems (NeurIPS)*, pages 8024–8035, 2019. 4, 5
- [34] Ilija Radosavovic, Raj Prateek Kosaraju, Ross B. Girshick, Kaiming He, and Piotr Dollár. Designing network design spaces. In *Conference on Computer Vision and Pattern Recognition (CVPR)*, pages 10425–10433, 2020. 5
- [35] Yiyou Sun, Chuan Guo, and Yixuan Li. React: Out-of-distribution detection with rectified activations. In *Conference on Neural Information Processing Systems (NeurIPS)*, pages 144–157, 2021. 1, 3, 5, 6
- [36] Yiyou Sun and Yixuan Li. DICE: leveraging sparsification for out-of-distribution detection. In *European Conference on Computer Vision (ECCV)*, volume 13684, pages 691–708, 2022. 3, 5, 6
- [37] Keke Tang, Chao Hou, Weilong Peng, Runnan Chen, Peican Zhu, Wenping Wang, and Zhihong Tian. CORES: convolutional response-based score for out-of-distribution detection. In *Computer Vision and Pattern Recognition (CVPR)*, pages 10916–10925, 2024. 5
- [38] Zhengzhong Tu, Hossein Talebi, Han Zhang, Feng Yang, Peyman Milanfar, Alan Bovik, and Yinxiao Li. Maxvit: Multi-axis vision transformer. In *European conference on computer vision (ECCV)*, pages 459–479, 2022. 5
- [39] Sagar Vaze, Kai Han, Andrea Vedaldi, and Andrew Zisserman. Open-set recognition: A good closed-set classifier is all you need. In *International Conference on Learning Representations (ICLR)*, 2022. 8
- [40] Haoqi Wang, Zhizhong Li, Litong Feng, and Wayne Zhang. Vim: Out-of-distribution with virtual-logit matching. In *Computer Vision and Pattern Recognition (CVPR)*, pages 4911–4920, 2022. 3, 4, 5, 6, 8
- [41] Hongxin Wei, Renchunzi Xie, Hao Cheng, Lei Feng, Bo An, and Yixuan Li. Mitigating neural network overconfidence with logit normalization. In *International Conference on Machine Learning (ICML)*, pages 23631–23644, 2022. 2
- [42] Jianxiong Xiao, James Hays, Krista A. Ehinger, Aude Oliva, and Antonio Torralba. SUN database: Large-scale scene recognition from abbey to zoo. In *Computer Vision and Pattern Recognition (CVPR)*, pages 3485–3492, 2010. 4, 5
- [43] Kai Xu, Rongyu Chen, Gianni Franchi, and Angela Yao. Scaling for training time and post-hoc out-of-distribution detection enhancement. In *International Conference on Learning Representations (ICLR)*, 2024. 3
- [44] Pingmei Xu, Krista A Ehinger, Yinda Zhang, Adam Finkelstein, Sanjeev R Kulkarni, and Jianxiong Xiao. Turkergaze: Crowdsourcing saliency with webcam based eye tracking. *arXiv preprint arXiv:1504.06755*, 2015. 5
- [45] Feng Xue, Zi He, Yuan Zhang, Chuanlong Xie, Zhenguo Li, and Falong Tan. Enhancing the power of OOD detection via sample-aware model selection. In *Computer Vision and Pattern Recognition (CVPR)*, pages 17148–17157, 2024. 1
- [46] Fisher Yu, Ari Seff, Yinda Zhang, Shuran Song, Thomas Funkhouser, and Jianxiong Xiao. Lsun: Construction of a large-scale image dataset using deep learning with humans in the loop. *arXiv preprint arXiv:1506.03365*, 2015. 5
- [47] Yeonguk Yu, Sungho Shin, Seongju Lee, Changhyun Jun, and Kyoobin Lee. Block selection method for using feature norm in out-of-distribution detection. In *Computer Vision and Pattern Recognition (CVPR)*, pages 15701–15711, 2023. 8, 1
- [48] Yue Yuan, Rundong He, Yicong Dong, Zhongyi Han, and Yilong Yin. Discriminability-driven channel selection for

- out-of-distribution detection. In *Computer Vision and Pattern Recognition (CVPR)*, pages 26171–26180, 2024. 1
- [49] Jingyang Zhang, Jingkang Yang, Pengyun Wang, Haoqi Wang, Yueqian Lin, Haoran Zhang, Yiyun Sun, Xuefeng Du, Yixuan Li, Ziwei Liu, Yiran Chen, and Hai Li. Openood v1.5: Enhanced benchmark for out-of-distribution detection. *arXiv preprint arXiv:2306.09301*, 2023. 1
- [50] Zihan Zhang and Xiang Xiang. Decoupling maxlogit for out-of-distribution detection. In *Conference on Computer Vision and Pattern Recognition (CVPR)*, pages 3388–3397, 2023. 2
- [51] Qinyu Zhao, Ming Xu, Kartik Gupta, Akshay Asthana, Liang Zheng, and Stephen Gould. Towards optimal feature-shaping methods for out-of-distribution detection. In *International Conference on Learning Representations (ICLR)*, 2024. 1, 3, 5, 6
- [52] Bolei Zhou, Àgata Lapedriza, Aditya Khosla, Aude Oliva, and Antonio Torralba. Places: A 10 million image database for scene recognition. *IEEE Transactions on Pattern Analysis and Machine Intelligence*, 40(6):1452–1464, 2018. 4, 5

CADRef: Robust Out-of-Distribution Detection via Class-Aware Decoupled Relative Feature Leveraging

Supplementary Material

7. Experiment Details

7.1. Dataset Settings

In our experiments, we perform OOD detection across two dataset scenarios. In the small-scale dataset scenario, we employ CIFAR-10 and CIFAR-100 as ID datasets, with SVHN, LSUN-R, LSUN-C, iSUN, Texture, and Places serving as the corresponding OOD datasets. In the large-scale dataset scenario, we use ImageNet-1k as the ID dataset, with OOD detection conducted on six datasets: iNaturalist, SUN, Places, Textures, OpenImage-O and ImageNet-O. Additionally, we also conduct extended experiments on SSB-hard and Ninco to further discuss the impact of the logit-based component. Table 8 provides detailed information of the datasets utilized in both scenarios.

	Dataset	# of Classes	# of Samples	Size
ID	CIFAR-10	10	10000	32×32
	CIFAR-100	100	10000	32×32
	ImageNet-1k	1000	50000	224×224
OOD (small-scale)	SVHN	–	26032	32×32
	LSUN-R	–	10000	32×32
	LSUN-C	–	10000	32×32
	iSUN	–	8925	32×32
	Texture	–	5640	32×32
	Places	–	10000	32×32
OOD (large-scale)	iNaturalist	–	10000	224×224
	SUN	–	10000	224×224
	Places	–	10000	224×224
	Texture	–	5640	224×224
	OpenImage-O	–	17632	224×224
	ImageNet-O	–	2000	224×224
	SSB-hard	–	49000	224×224
	Ninco	–	5878	224×224

Table 8. Details of ID/OOD datasets. Note that the third column is the number of test samples. All OOD dataset samples are processed to match the size of the corresponding ID dataset samples.

7.2. Hyperparameter Settings

The detailed hyperparameters of all baseline methods are listed in Table 9. For most baseline methods, we keep the same hyperparameters as the original paper. For methods that lack experiments on ImageNet-1k in the original work, we adopt the settings from the *ReAct* [35].

8. Detailed Experiment Results

For ImageNet-1k benchmark, we conduct extensive experiments using ResNet-50, RegNet-8GF, DenseNet-201, ViT-B/16, Swin-B, ConvNeXt-B, and MaxVit-B models to complete Table 3. All results are presented in Tables 10, 11, 12, 13, 14, 15, and 16, where *CARef* and *CADRef* consistently demonstrate superior performance across these models, highlighting the robustness of our methods.

9. Collapse of the feature norm

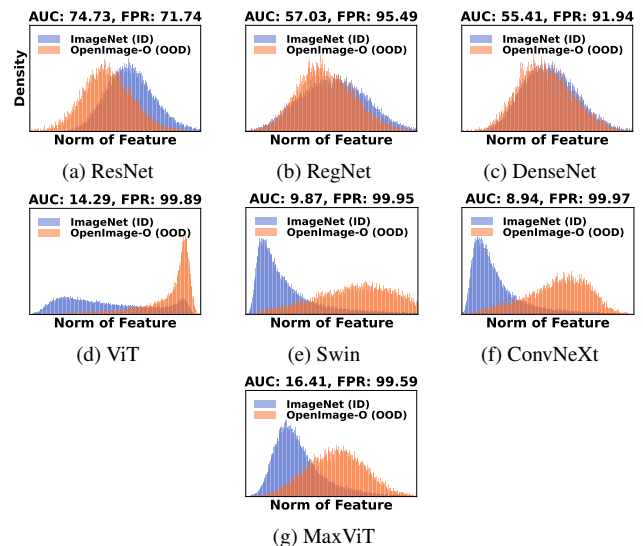


Figure 6. Comparison of feature ℓ_2 -norm across different models.

We also explore the challenges associated with using feature norm for OOD detection. According to the conclusion in [47], the feature norms of ID samples are generally larger than those of OOD samples. However, as shown in Figure 6, this conclusion holds only for ResNet. In RegNet and DenseNet, this method lacks discriminative power (with an AUROC of around 50%), and in other models, the conclusion is actually reversed.

Method	Configurable Hyperparameters	CIFAR-10	CIFAR-100	ImageNet-1k
<i>MSP</i>	None	–	–	–
<i>MaxLogit</i>	None	–	–	–
<i>ODIN</i>	T : temperature scaling ϵ : perturbation magnitude	$T = 1000$ $\epsilon = 0.0014$	$T = 1000$ $\epsilon = 0.002$	$T = 1000$ $\epsilon = 0.005$
<i>Energy</i>	T : temperature scaling	$T = 1$	$T = 1$	$T = 1$
<i>GEN</i>	M : top classes used in truncated sum γ : exponential scale	$M = 10$ $\gamma = 0.1$	$M = 10$ $\gamma = 0.1$	$M = 100$ $\gamma = 0.1$
<i>ReAct</i>	p : percentile for rectification threshold	$p = 90$	$p = 90$	$p = 90$
<i>DICE</i>	p : sparsity parameter	$p = 0.9$	$p = 0.7$	$p = 0.7$
<i>ViM</i>	D : dimension of principal space	$D = 171$	$D = 171$	$D = \begin{cases} 256 & \text{for MaxViT} \\ 1000 & \text{for ResNet} \\ 512 & \text{for others} \end{cases}$
<i>ASH-S</i>	p : pruning percentage	$p = 95$	$p = 90$	$p = 90$
<i>OptFS</i>	K : number of intervals	$K = 100$	$K = 100$	$K = 100$
<i>Ours</i>	None	–	–	–

Table 9. Hyperparameter settings for different OOD detection methods.

9.1. Score and error distribution for other methods

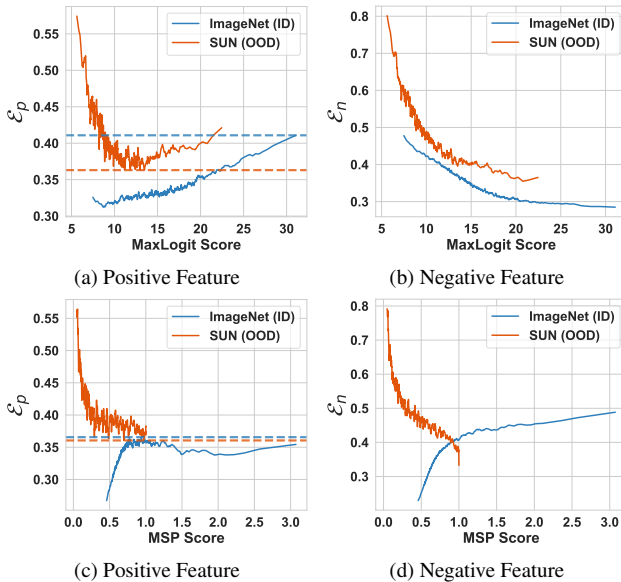


Figure 7. Score and error distribution of ID/OOD samples.

Figure 7 illustrates the score and error distributions for the *MSP* and *MaxLogit* methods. While the *MaxLogit* method demonstrates error trends consistent with the *Energy* and *GEN* methods, the *MSP* method exhibits a markedly different behavior. At higher S_{logit} values, *MSP* shows distinctly separated positive errors but significant overlap in negative errors, which fundamentally contradicts the *Error Scaling* component’s design principles. Consequently, integrating *MSP* as a logit-based component in *CADRef* leads to a detrimental impact, as substantiated by the results in Figure 5.

Methods	iNaturalist		SUN		Places		Textures		OpenImage-O		ImageNet-O		Average	
	AU↑	FP↓	AU↑	FP↓	AU↑	FP↓	AU↑	FP↓	AU↑	FP↓	AU↑	FP↓	AU↑	FP↓
<i>MSP</i>	88.42	52.73	81.75	68.58	80.63	71.59	80.46	66.15	84.98	63.60	28.61	100.00	74.14	70.44
<i>MaxLogit</i>	91.14	50.77	86.43	60.39	84.03	66.03	86.38	54.91	89.13	57.89	40.73	100.00	79.64	65.00
<i>ODIN</i>	87.00	52.33	86.57	53.49	85.30	58.64	86.51	46.08	86.65	52.76	43.63	98.65	79.28	60.32
<i>Energy</i>	90.59	53.96	86.73	58.28	84.12	65.43	86.73	52.30	89.12	57.23	41.79	100.00	79.85	64.53
<i>GEN</i>	92.44	45.76	85.52	65.54	83.46	69.24	85.41	59.24	89.31	60.44	43.59	100.00	79.95	66.70
<i>ReAct</i>	96.39	19.55	94.41	24.01	91.93	33.45	90.45	45.83	90.53	43.69	52.45	98.00	86.03	44.09
<i>DICE</i>	94.51	26.63	90.91	36.48	87.64	47.98	90.44	32.58	88.57	45.72	42.78	98.00	82.48	47.90
<i>ViM</i>	87.42	71.80	81.07	81.80	78.39	83.12	96.83	14.84	89.30	58.68	<u>70.77</u>	<u>84.85</u>	83.96	65.85
<i>ASH-S</i>	97.87	11.49	<u>94.02</u>	<u>27.96</u>	<u>90.98</u>	<u>39.83</u>	<u>97.60</u>	<u>11.97</u>	92.75	<u>32.77</u>	67.44	89.10	90.11	35.52
<i>OptFS</i>	96.88	16.79	93.13	35.31	90.42	44.78	95.74	23.08	<u>92.77</u>	37.68	59.94	97.20	88.15	42.47
<i>CARef</i>	96.54	17.46	89.51	44.89	85.41	57.64	97.94	10.15	92.57	37.73	77.66	77.60	<u>89.94</u>	40.91
<i>CADRef</i>	<u>96.90</u>	<u>16.08</u>	91.26	39.23	87.80	51.12	97.14	12.60	93.93	32.69	68.38	92.35	89.24	<u>40.68</u>

Table 10. Results of OOD detection on ImageNet-1k benchmark with ResNet-50. ↑ indicates that higher values are better, while ↓ indicates that lower values are better. All values are percentages, with the best and second-best results being **highlighted** and underlined, respectively.

Methods	iNaturalist		SUN		Places		Textures		OpenImage-O		ImageNet-O		Average	
	AU↑	FP↓	AU↑	FP↓	AU↑	FP↓	AU↑	FP↓	AU↑	FP↓	AU↑	FP↓	AU↑	FP↓
<i>MSP</i>	88.32	53.48	82.16	68.00	80.98	71.68	79.87	68.77	86.01	61.30	52.69	96.65	78.34	69.98
<i>MaxLogit</i>	90.01	51.89	86.32	57.56	84.02	64.45	82.71	61.24	89.59	51.53	57.64	95.80	81.71	63.75
<i>ODIN</i>	85.52	54.58	86.11	50.33	85.76	54.66	82.34	53.19	86.99	49.30	56.72	89.90	80.57	58.66
<i>Energy</i>	89.29	55.36	86.27	57.37	83.85	63.97	82.51	61.40	89.36	51.87	58.03	94.70	81.55	64.11
<i>GEN</i>	92.36	44.63	86.44	60.33	84.40	66.31	84.53	60.85	90.59	52.96	62.12	95.65	83.41	63.46
<i>ReAct</i>	96.04	21.72	94.85	24.55	91.71	36.38	87.26	56.80	87.96	47.03	61.91	91.35	86.62	46.30
<i>DICE</i>	88.83	56.48	84.19	62.09	80.05	74.33	80.13	64.18	81.65	62.26	52.65	94.00	77.92	68.89
<i>ViM</i>	90.88	58.04	85.31	70.72	82.12	75.84	97.35	12.23	91.95	48.58	<u>80.85</u>	<u>71.40</u>	88.08	56.13
<i>ASH-S</i>	96.49	18.52	91.00	<u>35.15</u>	86.84	<u>50.60</u>	97.12	<u>13.40</u>	91.07	<u>35.58</u>	73.71	74.80	<u>89.37</u>	38.01
<i>OptFS</i>	<u>96.06</u>	<u>20.96</u>	<u>92.03</u>	40.58	<u>88.30</u>	51.62	95.90	22.96	<u>92.33</u>	37.47	71.19	84.20	89.30	42.97
<i>CARef</i>	93.07	41.97	86.21	57.28	81.48	72.04	<u>97.26</u>	15.00	90.21	47.77	81.38	70.00	88.27	50.68
<i>CADRef</i>	95.31	28.13	90.29	44.08	86.73	58.14	97.20	14.02	93.87	34.70	78.15	75.00	90.26	<u>42.34</u>

Table 11. Results of OOD detection on ImageNet-1k benchmark with RegNet-8GF. ↑ indicates that higher values are better, while ↓ indicates that lower values are better. All values are percentages, with the best and second-best results being **highlighted** and underlined, respectively.

Methods	iNaturalist		SUN		Places		Textures		OpenImage-O		ImageNet-O		Average	
	AU↑	FP↓	AU↑	FP↓	AU↑	FP↓	AU↑	FP↓	AU↑	FP↓	AU↑	FP↓	AU↑	FP↓
<i>MSP</i>	89.83	44.80	82.22	65.22	81.13	68.86	79.40	67.02	85.21	61.93	48.78	97.95	77.76	67.63
<i>MaxLogit</i>	92.12	40.68	85.91	55.85	83.83	62.12	83.41	58.31	88.31	55.05	53.35	97.35	81.16	61.56
<i>ODIN</i>	89.95	42.93	84.09	55.57	83.01	59.93	81.45	54.85	84.70	56.80	50.21	94.40	78.90	60.75
<i>Energy</i>	91.47	43.76	85.97	53.85	83.68	61.42	83.44	56.61	87.95	55.92	54.04	95.95	81.09	61.25
<i>GEN</i>	93.37	37.92	85.77	59.34	84.03	64.53	83.78	60.69	89.24	58.20	58.18	97.40	82.39	63.01
<i>ReAct</i>	88.65	51.99	89.55	51.38	85.92	61.57	81.49	60.83	74.19	68.20	50.97	91.10	78.46	64.18
<i>DICE</i>	91.73	39.18	86.76	48.13	82.29	60.72	83.85	53.28	81.62	59.35	48.94	93.60	79.20	59.04
<i>ViM</i>	82.69	85.18	73.99	91.50	72.87	91.43	94.66	26.13	87.21	66.06	<u>76.58</u>	<u>75.64</u>	81.33	72.66
<i>ASH-S</i>	96.18	20.51	90.58	39.42	87.54	50.40	93.81	26.13	92.28	37.42	64.97	88.95	87.56	43.80
<i>OptFS</i>	94.61	28.62	<u>90.08</u>	<u>46.12</u>	<u>86.18</u>	<u>56.28</u>	95.17	26.32	90.23	46.91	73.21	83.00	<u>88.25</u>	47.88
<i>CARef</i>	92.94	36.18	84.16	60.12	78.68	72.13	96.43	<u>18.99</u>	87.01	54.50	80.08	73.60	86.55	52.59
<i>CADRef</i>	<u>95.41</u>	<u>24.59</u>	89.17	47.19	85.03	58.96	<u>96.39</u>	16.68	<u>91.57</u>	<u>42.85</u>	74.27	81.20	88.64	<u>45.25</u>

Table 12. Results of OOD detection on ImageNet-1k benchmark with DenseNet-201. ↑ indicates that higher values are better, while ↓ indicates that lower values are better. All values are percentages, with the best and second-best results being **highlighted** and underlined, respectively.

Methods	iNaturalist		SUN		Places		Textures		OpenImage-O		ImageNet-O		Average	
	AU↑	FP↓	AU↑	FP↓	AU↑	FP↓	AU↑	FP↓	AU↑	FP↓	AU↑	FP↓	AU↑	FP↓
<i>MSP</i>	88.18	51.42	80.88	66.65	80.37	68.49	82.96	60.47	84.81	59.84	58.79	90.85	79.33	66.29
<i>MaxLogit</i>	85.27	52.14	76.28	66.86	75.03	69.19	81.64	56.57	81.53	58.72	54.31	88.94	75.68	65.40
<i>ODIN</i>	71.50	94.86	56.56	95.31	56.12	95.49	66.32	92.18	62.79	94.79	55.43	93.35	61.45	94.33
<i>Energy</i>	79.27	63.93	70.16	72.81	68.39	74.35	79.24	58.45	76.44	64.83	52.71	87.00	71.04	70.23
<i>GEN</i>	92.91	40.05	<u>85.03</u>	<u>61.06</u>	83.49	<u>64.22</u>	87.97	50.69	89.36	52.53	67.44	88.90	84.37	<u>59.58</u>
<i>ReAct</i>	85.99	65.07	78.93	72.38	77.48	73.84	84.62	57.09	84.21	64.58	66.69	87.00	79.65	69.99
<i>DICE</i>	74.54	90.41	65.23	94.51	64.79	93.05	77.34	84.04	77.28	83.01	70.75	<u>86.05</u>	71.65	88.51
<i>ViM</i>	97.18	12.55	83.99	56.77	81.48	58.98	88.92	46.48	92.44	38.11	76.29	83.25	86.72	49.36
<i>ASH-S</i>	6.68	99.99	16.70	99.73	18.32	99.65	24.13	99.13	14.04	99.84	28.46	99.40	18.06	99.62
<i>OptFS</i>	89.94	55.59	84.19	66.36	82.70	68.39	86.46	56.60	88.20	59.86	71.85	89.15	83.89	65.99
<i>CARef</i>	<u>94.07</u>	<u>36.59</u>	84.83	66.92	83.03	68.36	<u>89.28</u>	52.57	<u>91.54</u>	<u>50.32</u>	78.31	88.14	<u>86.84</u>	60.48
<i>CADRef</i>	93.81	38.45	85.12	65.85	<u>83.28</u>	67.91	89.59	<u>49.78</u>	91.52	50.44	<u>78.12</u>	87.85	86.91	60.05

Table 13. Results of OOD detection on ImageNet-1k benchmark with ViT-B/16. ↑ indicates that higher values are better, while ↓ indicates that lower values are better. All values are percentages, with the best and second-best results being **highlighted** and underlined, respectively.

Methods	iNaturalist		SUN		Places		Textures		OpenImage-O		ImageNet-O		Average	
	AU↑	FP↓	AU↑	FP↓	AU↑	FP↓	AU↑	FP↓	AU↑	FP↓	AU↑	FP↓	AU↑	FP↓
<i>MSP</i>	87.00	51.68	80.53	66.52	80.69	67.79	78.46	66.20	81.78	62.13	58.38	88.40	77.81	67.12
<i>MaxLogit</i>	79.86	55.48	72.23	67.86	71.97	69.54	73.98	61.93	71.08	65.52	56.00	85.75	70.85	67.68
<i>ODIN</i>	58.88	90.31	51.06	92.18	48.57	93.24	64.36	86.61	52.42	92.10	56.00	91.70	55.22	91.02
<i>Energy</i>	68.57	72.55	63.08	78.54	62.48	78.92	69.58	65.95	60.23	76.13	55.13	83.65	63.18	75.96
<i>GEN</i>	92.69	32.94	<u>85.02</u>	56.61	84.06	59.95	85.61	49.93	87.18	48.66	67.77	83.90	83.72	55.33
<i>ReAct</i>	88.72	59.29	81.46	69.10	80.87	70.79	84.07	57.83	85.90	61.58	70.45	80.85	81.91	66.57
<i>DICE</i>	23.13	97.70	42.48	91.57	33.91	94.74	73.15	63.22	45.55	86.66	56.50	86.65	45.79	86.76
<i>ViM</i>	<u>93.60</u>	44.56	80.12	71.10	77.96	71.82	83.96	64.64	92.10	<u>46.36</u>	76.03	83.80	83.96	63.63
<i>ASH-S</i>	10.69	99.81	20.18	99.36	21.37	99.59	18.41	98.65	11.94	99.84	32.52	98.85	19.18	99.35
<i>OptFS</i>	90.71	54.98	84.86	67.93	<u>83.94</u>	68.63	85.10	61.68	90.34	51.19	73.28	85.75	84.71	65.03
<i>CARef</i>	93.57	39.78	84.83	66.72	83.25	68.68	<u>88.74</u>	<u>49.86</u>	92.55	43.52	<u>78.57</u>	83.35	<u>86.92</u>	58.65
<i>CADRef</i>	93.77	<u>37.87</u>	85.12	<u>64.23</u>	83.57	<u>66.71</u>	89.08	47.38	<u>92.32</u>	46.63	78.76	<u>81.45</u>	87.10	<u>57.38</u>

Table 14. Results of OOD detection on ImageNet-1k benchmark with Swin-B. ↑ indicates that higher values are better, while ↓ indicates that lower values are better. All values are percentages, with the best and second-best results being **highlighted** and underlined, respectively.

Methods	iNaturalist		SUN		Places		Textures		OpenImage-O		ImageNet-O		Average	
	AU↑	FP↓	AU↑	FP↓	AU↑	FP↓	AU↑	FP↓	AU↑	FP↓	AU↑	FP↓	AU↑	FP↓
<i>MSP</i>	89.69	44.35	79.28	63.37	78.41	67.02	73.77	65.76	83.40	58.48	52.85	92.45	76.23	65.24
<i>MaxLogit</i>	83.32	57.91	69.83	72.02	68.44	74.92	65.72	70.88	74.08	68.10	51.18	92.10	68.76	72.66
<i>ODIN</i>	63.62	81.28	47.54	91.28	47.73	90.28	43.43	93.49	52.75	88.20	51.48	91.45	51.09	89.33
<i>Energy</i>	57.94	90.10	51.17	94.53	50.85	92.84	52.87	87.26	54.62	88.78	50.00	93.00	52.91	91.09
<i>GEN</i>	94.86	25.69	84.78	52.70	83.04	59.18	80.10	55.21	89.37	46.11	64.02	90.50	82.69	<u>54.90</u>
<i>ReAct</i>	87.94	68.80	78.51	78.02	77.07	79.42	76.45	71.57	83.30	73.30	65.61	90.10	78.15	76.87
<i>DICE</i>	20.82	98.55	41.27	93.95	34.27	96.24	71.72	69.92	47.62	88.50	54.99	91.45	45.12	89.77
<i>ViM</i>	93.63	40.84	85.00	59.57	82.17	<u>61.76</u>	86.79	52.41	91.36	45.33	66.46	91.50	84.24	58.57
<i>ASH-S</i>	3.79	99.91	10.77	99.56	14.87	99.02	33.22	96.20	17.33	98.67	41.80	96.00	20.30	98.23
<i>OptFS</i>	92.20	46.02	85.96	61.69	<u>85.10</u>	64.02	86.11	54.32	91.02	49.68	69.97	91.30	85.06	61.17
<i>CARef</i>	<u>94.81</u>	<u>29.79</u>	87.37	<u>58.04</u>	85.40	63.09	90.04	45.09	93.39	38.82	76.70	<u>89.70</u>	87.95	54.09
<i>CADRef</i>	94.50	33.08	<u>86.84</u>	60.16	84.92	65.09	<u>89.27</u>	<u>49.17</u>	<u>92.85</u>	<u>44.85</u>	<u>76.49</u>	89.15	87.48	56.92

Table 15. Results of OOD detection on ImageNet-1k benchmark with ConvNeXt-B. ↑ indicates that higher values are better, while ↓ indicates that lower values are better. All values are percentages, with the best and second-best results being **highlighted** and underlined, respectively.

Methods	iNaturalist		SUN		Places		Textures		OpenImage-O		ImageNet-O		Average	
	AU \uparrow	FP \downarrow	AU \uparrow	FP \downarrow	AU \uparrow	FP \downarrow	AU \uparrow	FP \downarrow	AU \uparrow	FP \downarrow	AU \uparrow	FP \downarrow	AU \uparrow	FP \downarrow
<i>MSP</i>	89.04	49.30	82.99	61.46	81.95	64.91	84.33	57.32	86.25	55.89	57.62	92.10	80.36	63.50
<i>MaxLogit</i>	90.54	37.76	80.88	55.30	78.52	61.36	84.81	45.18	82.97	51.04	45.37	93.05	77.18	57.28
<i>ODIN</i>	75.26	75.28	60.07	83.23	55.45	86.82	75.86	68.35	64.37	82.93	56.56	92.15	64.60	81.46
<i>Energy</i>	88.79	43.36	76.62	62.14	73.14	68.26	82.78	46.37	76.69	59.99	40.03	94.65	73.01	62.46
<i>GEN</i>	94.41	28.58	87.36	50.14	85.44	56.12	89.07	42.70	91.18	40.67	65.53	<u>89.10</u>	85.50	51.22
<i>ReAct</i>	80.15	68.51	62.81	81.64	58.01	86.14	74.11	63.78	66.68	76.46	40.92	96.90	63.78	78.91
<i>DICE</i>	80.47	66.61	67.78	76.60	63.51	83.42	75.38	60.53	63.90	75.45	28.18	98.10	63.20	76.78
<i>ViM</i>	<u>95.26</u>	27.62	80.81	63.22	75.83	67.38	<u>91.30</u>	41.21	93.06	37.38	75.79	84.55	85.34	53.56
<i>ASH-S</i>	47.01	90.66	65.40	80.89	65.26	84.48	65.48	73.95	49.06	89.75	39.32	98.05	55.26	86.30
<i>OptFS</i>	81.08	63.02	79.33	68.12	78.40	71.79	77.54	66.22	79.82	65.97	54.35	89.95	75.09	70.84
<i>CARef</i>	95.11	<u>26.30</u>	<u>87.61</u>	54.21	<u>85.49</u>	59.71	91.18	<u>38.62</u>	93.30	<u>35.97</u>	<u>73.52</u>	89.70	<u>87.70</u>	<u>50.75</u>
<i>CADRef</i>	95.35	24.23	87.82	<u>52.19</u>	85.68	<u>58.26</u>	91.38	37.06	<u>93.29</u>	35.75	72.87	89.45	87.73	49.49

Table 16. Results of OOD detection on ImageNet-1k benchmark with MaxViT-T. \uparrow indicates that higher values are better, while \downarrow indicates that lower values are better. All values are percentages, with the best and second-best results being **highlighted** and underlined, respectively.